Received: 24 June 2020 | Revised: 9 November 2020 | Accepted: 1 December 2020

DOI: 10.1111/jace.17629

Journal of the American Ceramic Society

ORIGINAL ARTICLE

Structure-property relations in crack-resistant alkaline-earth aluminoborosilicate glasses studied by solid state NMR

Millena Lograd[1] | Hellmut Eckert[1,2] | Tetsuya Murata[3] | Shingo Nakane[3] | Hiroki Yamazaki[3]

[1]Instituto de Física de São Carlos, Universidade de São Paulo, São Carlos, Brazil

[2]Institut für Physikalische Chemie, Westfälische Wilhelms-Universität Münster, Münster, Germany

[3]Nippon Electric Glass Co., Ltd., Otsu, Shiga, Japan

Correspondence
Hellmut Eckert, Instituto de Física de São Carlos, Universidade de São Paulo, CP 369, 13566-590, São Carlos, SP, Brazil.
Email: eckerth@uni-muenster.de

Funding information
Fundação de Amparo à Pesquisa do Estado de São Paulo, Grant/Award Number: 2013/07793-6

Abstract

The effect of the average ionic potential $\xi = Ze/r$ of the network modifier cations on crack initiation resistance (*CR*) and Young's modulus *E* has been measured for a series of alkaline-earth aluminoborosilicate glasses with the compositions $60SiO_2$–$10Al_2O_3$–$10B_2O_3$–$(20-x)M_{(2)}O$–$xM'O$ ($0 \leq x \leq 20$; M, M' = Mg, Ca, Sr, Ba, Na). Systematic trends indicating an increase of *CR* with increasing ionic potential, ξ, have been correlated with structural properties deduced from the NMR interaction parameters in ^{29}Si, ^{27}Al, ^{23}Na, and ^{11}B solid state NMR. ^{27}Al NMR spectra indicate that the aluminum atoms in these glasses are essentially all four-coordinated, however, the average quadrupolar coupling constant $<C_Q>$ extracted from lineshape analysis increases linearly with increasing average ion potential computed from the cation composition. A similar linear correlation is observed for the average ^{29}Si chemical shift, whereas the fraction of four-coordinate boron decreases linearly with increasing ξ. Altogether the results indicate that in pure alkaline-earth boroaluminosilicate glasses the crack resistance/*E*-modulus trade-off can be tailored by the alkaline-earth oxide inventory. In contrast, the situation looks more complicated in glasses containing both Na_2O and the alkaline-earth oxides MgO, CaO, SrO, and BaO. For $60SiO_2$–$10Al_2O_3$–$10B_2O_3$–$10MgO$–$10Na_2O$ glass, the NMR parameters, interpreted in the context of their correlations with ionic potentials, are consistent with a partial network former role of the MgO component, enhancing crack resistance. Altogether the presence of MgO in aluminoborosilicate glasses helps overcome the trade-off issue between high crack resistance and high elasticity modulus present in borosilicate glasses, thereby offering additional opportunities for the design of glasses that are both very rigid and very crack resistant.

KEYWORDS

glass, magnesium oxide, mechanical properties, nuclear magnetic resonance, structure

1 | INTRODUCTION

Ultrastrong glasses with high crack initiation resistance are of great interest for the optimization of the surface properties of modern household devices. New oxide glass formulations for improving the mechanical strengths without compromising other physical properties are under continuous development.[1–8] The different composition requirements for preparing glasses with maximum hardness on the one hand and maximum crack initiation resistance on the other has been an important issue in this regard. While high packing densities promote hardness, they tend to limit the ability of deflecting mechanical stresses leading to lower crack resistances. Numerous silicate,[2] borosilicate,[3,4] aluminosilicate,[5] and aluminoborate glass compositions have been explored in an effort to find a good compromise between these conflicting demands.[6] A promising approach for overcoming this dichotomy has been the incorporation of the high-field strength cations Mg^{2+} and Al^{3+} into silicate glass formulations. For example, in the Al_2O_3–SiO_2 glass system an increase in the Al_2O_3 content has the effect of increasing the hardness and crack initiation resistance simultaneously. On the basis of NMR data, this effect has been rationalized in terms of increasing concentrations of Al occurring in five- and sixfold coordination.[7] Likewise, in a series of alkaline-earth aluminoborate glasses of composition $25RO–20Al_2O_3–55B_2O_3$ (R = Mg, Ca, Sr, Ba) hardness and crack initiation resistance increase in parallel with decreasing size of the alkaline-earth metal ion.[8] This effect is correlated with a significant decrease in the tendency of these glasses to contain four-coordinate boron species. Based on the latter result the prospect of tuning the mechanical properties of boroaluminosilicate glasses via the alkaline-earth metal oxide inventory appears attractive. To monitor the structural origins of this evolution, nuclear magnetic resonance has already provided some important insights into this matter.[4–6,8,9] In aluminosilicate and aluminoborate glasses, crack initiation resistance was shown to increase with increasing average coordination number (presence of higher-coordinated aluminum species).[5,7] In the alkaline-earth aluminoborate glasses of Ref. [8] these structural changes have been monitored exactly. Furthermore, recently a synergistic effect upon crack initiation resistance was noted for glasses containing comparable amounts of both network formers Al_2O_3 and B_2O_3.[9] While a large number of multinuclear NMR results on alkali- and alkaline-earth aluminosilicate and aluminoborosilicate glasses can be found in the literature,[9–28] work conducted by the Stebbins group has pointed out the significance of the ability of the cations to polarize their local environment upon physical properties and NMR observables in silicate glasses.[11,12,16]. Two quantities can be used in this context: (a) the average *ionic potential* is defined by $\xi = \sum_i f_i z_i e / r_i$, where z_i and r_i are the charge and the radius of the cation i, f_i is its fractional contribution to the network modifier inventory, and $e = 1.602 \times 10^{-19}$C. Alternatively *cation field strength* can be used, which is the gradient of the ionic potential. In this study, we use the ionic potential concept to explore the structure/function relation within the present compositional series of aluminoborosilicate glasses by systematically changing the alkaline-earth ion inventory. The particular motivation for this work was to gain further insight into the structural role of magnesium in crack-resistant glasses and its effect on physical properties. Can it be understood in terms of a regular cation field strength effect or must we consider a potential network former role of this element? To clarify this issue, we have conducted a structural study on the systems $60SiO_2–10Al_2O_3–10B_2O_3–10Na_2O–10MO$ (M = Mg,[9] Ca, Sr, Ba) and $60SiO_2–10Al_2O_3–10B_2O_3–(20–x)MO–xMgO$ (M = Ca, Sr, Ba), combining results from ^{11}B, ^{27}Al, ^{23}Na, and ^{29}Si solid state NMR with physical property measurements.

2 | EXPERIMENTAL PROCEDURE

2.1 | Glass design, preparation and characterization

With the objective of systematically varying the cationic ion potential, a series of glasses with composition $60SiO_2–10Al_2O_3–10B_2O_3–(20–x)M_{(2)}O–xM_{(2)}'O$ ($0 \le x \le 20$; M, M' = Mg, Ca, Sr, Ba, Na) was prepared. Within this series of glasses, the average ionic potential of the cationic charge compensator was systematically varied by changing the alkaline-earth cationic composition. Using the values of 86, 114, 132, 149, and 116 pm (crystal ionic radii as listed in Ref. [29]) we calculate ionic potentials of 3.72, 2.81, 2.42, 2.15, and 1.38×10^{-9}C/m, for Mg^{2+}, Ca^{2+}, Sr^{2+}, Ba^{2+}, and Na^+, respectively. In glasses with mixed cation compositions, weighed averages were calculated (see Table 1).

Table 1 summarizes the glass compositions and the physical properties measured. The batches were mixed thoroughly and melted in 500 cm^3 Pt crucibles at 1100°C–1650°C for about 22 h in an electric furnace. The melting temperature for each composition was chosen according to the viscosity of the melt. After the melting period the glass melts were poured onto a carbon plate, and then placed in an electric furnace to cool slowly. Glass transition temperatures (T_g:±2°C), were determined using a dilatometer. The cooled glass was heated up to a temperature of (T_g +30°C), held for 30 min, and then cooled by 3°C/min to obtain annealed glasses. Crystallization or phase separation was not observed using a microscope in all the samples prepared in this study. The composition of each sample was analyzed

TABLE 1 Compositions (in mole %), crack resistance, *CR*, glass transition temperature, T_g(±2°C) density, ρ (±0.01 g/cm^3) molar volume, *V*, elasticity (Young's modulus *E*(±1 GPa), and average ionic potential ξ of the network modifier cations in the $60SiO_2$–$10Al_2O_3$–$10B_2O_3$–$(20-x)M_{(2)}O$–$xM_{(2)}$'O ($0 \le x \le 20$; M, M' = Mg, Ca, Sr, Ba, Na) glasses under study

MgO	CaO	SrO	BaO	Na_2O	*CR* (gf)	T_g (°C)	ρ (g/cm^3)	*V* (cm^3)	*E* (GPa)	$\xi\times10^9$C/m
	20				250 ± 40	698	2.52	25.56	80	2.81
5	15				1140 ± 180	692	2.49	25.55	79	3.03
10	10				1770 ± 90	694	2.47	25.44	81	3.27
		20			80 ± 5	696	2.83	26.12	79	2.42
5		15			180 ± 10	690	2.73	25.92	77	2.75
10		10			1700 ± 60	694	2.62	25.80	78	3.07
			20		60 ± 10	677	3.11	26.97	75	2.15
5			15		160 ± 10	676	2.92	26.79	73	2.54
10			10		1440 ± 50	682	2.75	26.39	74	2.94
10				10	1700 ± 40	604	2.40	26.44	69	2.55
	10			10	650 ± 60	598	2.47	26.32	74	2.10
		10		10	90 ± 10	597	2.65	26.33	76	1.90
			10	10	60 ± 10	587	2.80	26.69	77	1.77
				20	1000 ± 60	562	2.46	26.67	73	1.38

using X-ray fluorescence. These analyses confirmed that the glass compositions are close to the batch compositions (see Table S1, Supporting Materials). Samples of the glasses were ground, lapped with Al_2O_3 slurry, and then finished with cerium oxide to get optically smooth surfaces, which were used for the following indentation tests. Further physical properties measured include density (ρ:±0.01 g/cm^3) and Young's modulus (*E*:±1 GPa). Density was measured using Archimedes's method. Young's modulus was determined by a resonance method. The crack resistance value (*CR*) was measured by Vickers indentation tests.[4,30,31] The glass sample was exposed to a Vickers diamond indenter in air (25°C, 30% relative humidity), for a loading time of 15 s, and the corners where radial cracks appeared were counted after 15 s after unloading using an optical microscope. When the glass sample is indented, various types of cracks form around the indenter. Only radial cracks are counted for determining crack resistance, because the cracks normal to the glass surface are critical to fracture of glass. The percentage of crack initiation was determined as the ratio of the number of the corners with the cracks to the total number of the corners of indentations. The applied load was increased step-by-step and twenty indentations were made for each applied load. The load at which the percentage would be 50% is determined as "crack resistance", *CR*.

2.2 | Solid state NMR

Single resonance ^{11}B, ^{23}Na, ^{27}Al, and ^{29}Si MAS-NMR spectra were recorded at 5.7 and 14.1 T using Agilent DD2 and Bruker Avance Neo 600 MHz spectrometers, respectively, equipped with commercial MAS-NMR probes operated under the conditions specified in Table 2. Chemical shifts are reported relative to aqueous solutions of 0.1 M NaCl and 1 M $Al(NO_3)_3$, liquid TMS, and BF_3-Et_2O using solid secondary standards of NaCl, AlF_3, tetrakis-(trimethylsilyl) silane and BPO_4. ^{11}B MAS-NMR spectra were fitted with the DMfit program,[32] assuming second-order perturbation theory for the simulation of the three-coordinated boron species, and Gauss-Lorentz curves for the four-coordinated boron species. No intensity correction was done for satellite transition MAS sideband intensity contributing to the central ^{11}B MAS-NMR line of the $B^{(4)}$ units. The ^{23}Na and ^{27}Al MAS-central transition spectra were fitted according to the Czjzek model,[33] implemented within the DMfit data processing and simulation program.[32] ^{29}Si MAS-NMR spectra were recorded in 7.5 mm rotors, using 90° pulses of 5.5 μs length and a relaxation delay of 1400 s.

TABLE 2 Typical measurement conditions used for the glasses under study: resonance frequency ν_0, excitation pulse length t_p, relaxation delay *D*1, MAS spinning frequency ν_r, and number of scans *NS*

Nucleus	ν_0/MHz	t_p/μs	*D*1/s	ν_r/kHz	*NS*
^{11}B	192.6	0.2	1.0	25.0	3000
	77.8	0.1	1.0	20.0	8000
^{23}Na	158.8	0.3	1.0	25.0	2000
^{27}Al	156.4	0.1	1.0	25.0	4000
^{29}Si	48.2	5.5	1400	5.0	48

3 | RESULTS AND DATA ANALYSIS

3.1 | Composition-dependent bulk properties

Table 1 summarizes the bulk physical properties measured. Only moderate changes are observed in the *E*-moduli and molar volumes. Overall V_M tends to increase and E tends to decrease with increasing size of the modifier ion as expected. In the Na_2O-MO-containing samples, the molar volumes of the intermediate compositions are found in-between the molar volumes of the corresponding end member compositions, but no systematic trends can be found for the elasticity moduli. Regarding crack resistance, the following trends can be noted:

1. In the all-alkaline-earth systems successive substitution of the alkaline-earth oxide by its homologue MgO systematically increases Log(*CR*) linearly with increasing average ionic potential of the cation inventory (Figure 1a).
2. For the glass with composition $60SiO_2$–$10Al_2O_3$–$10B_2O_3$–$10Na_2O$–10MO (M = Mg, Ca, Sr, Ba), Log(*CR*) increases linearly with increasing average ionic potential of the cation inventory, reflecting the analogous trends observed in alkaline-free glasses discussed above (Figure 1b).
3. For the glasses with composition $60SiO_2$–$10Al_2O_3$–$10B_2O_3$–20MO, the successive substitution of Mg, Ca, Sr, or Ba with 2Na, $60SiO_2$–$10Al_2O_3$–$10B_2O_3$–$(20-x)$MO–xNa_2O, shows different characteristics. In the case of MgO, Log(*CR*) increases with increasing average ionic potential. In contrast, in the case of CaO, SrO, and BaO, Log(*CR*) decreases with increasing average ionic potential. Thus, for the case of the $Na_2O \rightarrow MO$ substitution, no clear relationship between Log(*CR*) and average ionic potential is found (Figure 1c). Figure 1 indicates that in those glasses in which the modifier inventory comprises $20Na_2O$, $10MgO$–$10Na_2O$, and $10CaO$–$10Na_2O$, Log(*CR*) is higher than predicted from the monotonic

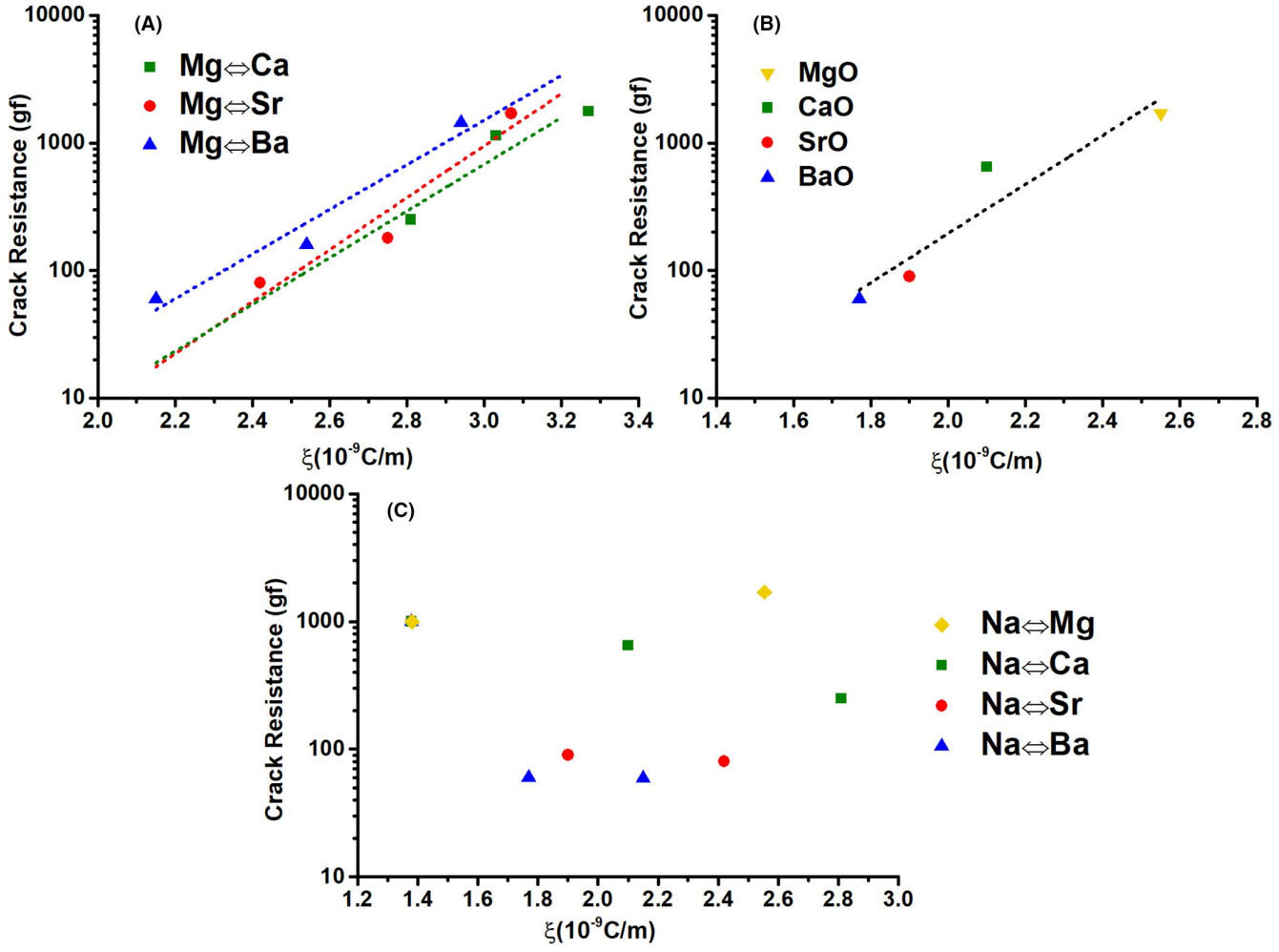

FIGURE 1 Correlation of the crack resistance with the average ionic potential for glasses in the systems: (A) $60SiO_2$–$10B_2O_3$–$10Al_2O_3$–$(20-x)$MO–xMgO (x = 0, 5, 10) (M = Ca, Sr, Ba), (B) $60SiO_2$–$10B_2O_3$–$10Al_2O_3$–$10Na_2O$–10MO (M = Mg, Ca, Sr, Ba), and (C) $60SiO_2$–$10B_2O_3$–$10Al_2O_3$–$(20-x)$MO–xNa_2O (M = Mg, Ca, Sr, Ba) [Color figure can be viewed at wileyonlinelibrary.com]

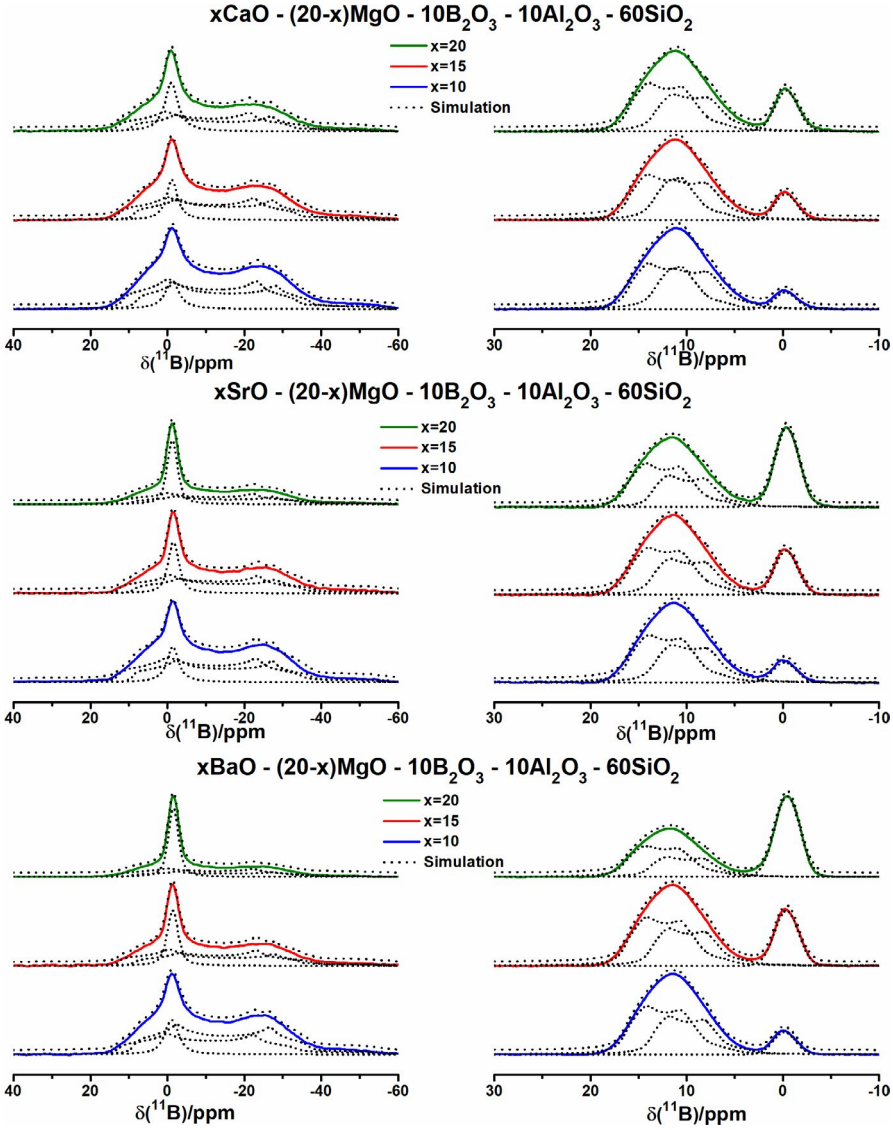

FIGURE 2 ^{11}B MAS-NMR spectra measured at 5.7 T (left) and at 14.1 T (right), of glasses in the system $60SiO_2$–$10B_2O_3$–$10Al_2O_3$–$(20-x)$ MO–xMgO (M = Ca, Sr, Ba, $x = 0, 5, 10$) along with their simulations using the DMFit program (dashed curves) [Color figure can be viewed at wileyonlinelibrary.com]

correlation with the ion potential followed by all the other glasses.

3.2 | ^{11}B MAS-NMR

Figures 2 and 3 summarize the ^{11}B MAS-NMR results of the glasses under study. Measurements were done at two different magnetic field strengths (14.1 T and 5.7 T). The spectra show two distinct boron coordination environments: the dominant fraction of the boron species is three-coordinate (B(III)) and characterized by a typical second-order quadrupolar lineshape, which is strongly field-dependent. The minority boron species is four-coordinate (B(IV)), producing a simple Gaussian lineshape near zero ppm. For these species, the nuclear electric quadrupolar interaction is too weak to be analyzed from the ^{11}B MAS-NMR lineshapes. The simulation parameters are listed in Table 3. To obtain consistent simulation parameters for the spectra observed at both magnetic field strengths, it was necessary to assume two distinct three-coordinate boron species: one component with an isotropic chemical shift δ_{iso}^{cs} near 14 ± 1 ppm (B^3(III)-1) and one component with δ_{iso}^{cs} near 17 ppm (B^3(III)-2). Both components are characterized by nuclear electric quadrupolar coupling constants C_Q near 2.6 ± 0.1 MHz and asymmetry parameter η_Q near 0.30 ± 0.05. These parameters are typical for symmetrical $BO_{3/2}$ (B^3) units featuring three bridging oxygen atoms. In the notation used here, the Latin numeral denotes the coordination number and the superscript specifies the number of bridging oxygen atoms. The Latin numeral is omitted whenever the coordination number of the network former unit is obvious from context,

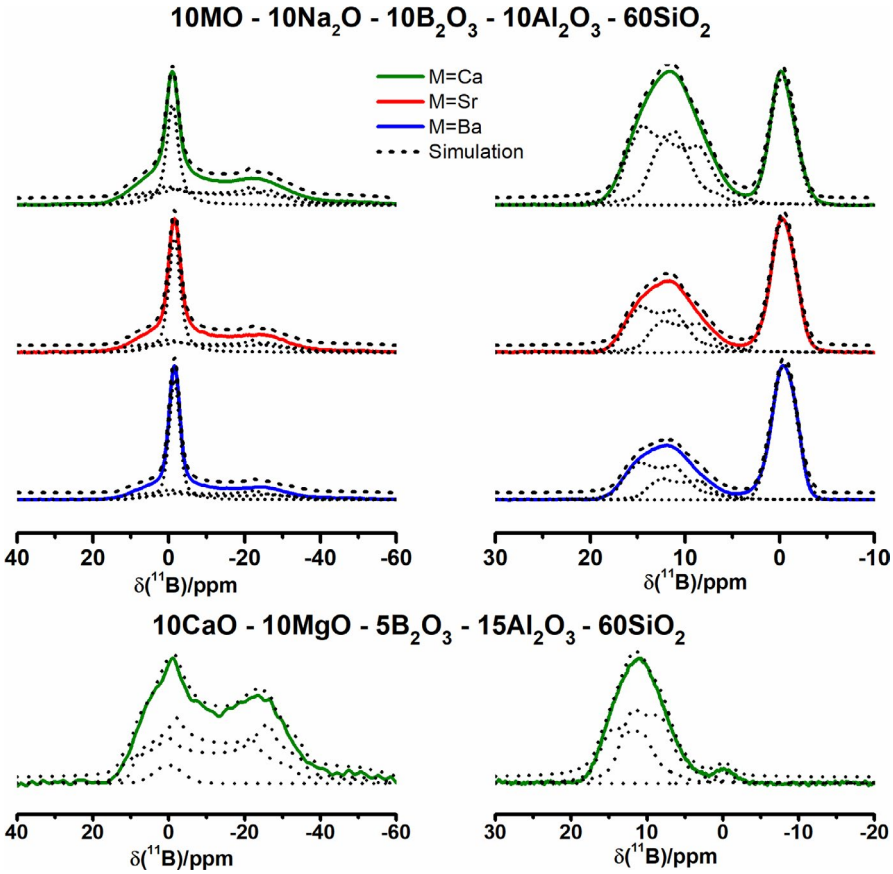

FIGURE 3 ^{11}B MAS-NMR spectra measured at 5.7 T (left) and at 14.1 T (right), of glasses in the system $60SiO_2$–$10B_2O_3$–$10Al_2O_3$–$10Na_2O$–10MO (M = Ca, Sr, Ba) and of $60SiO_2$–$5B_2O_3$–$15Al_2O_3$–10CaO–10MgO glass along with their simulations using the DMFit program [Color figure can be viewed at wileyonlinelibrary.com]

for example all Si^n-species discussed here are of the Si(IV) type. Isotropic chemical shifts and nuclear electric quadrupole coupling constants show no significant compositional trends. While the two B^3 sites may be assignable to units outside of and within ring structures as previously shown for glassy B_2O_3,[34] there may be alternative assignments, based on B^3(III)–O–Si versus B^3(III)–O–B linking.[35] Also, it needs to be pointed out that the deconvolution into two types of B^3(III) units is only the simplest possible model, and more complex distributions of chemical shift and electric field gradient tensor values might be able to reproduce the field-dependent data equally well. Nevertheless, the fractions of three- and four-coordinated boron species obtained by these simulations are accurate and consistent at the two magnetic field strengths measured. The existence of at least two distinct B^3(III) sites consistent with the MAS-NMR fit is also confirmed by a TQMAS experiment (see Figure S1, Supporting Materials Section). Table 3 reveals some striking compositional dependences of the fraction of four-coordinate boron, N_4:

1. Partial replacement of Na_2O by alkaline-earth oxide leads to a reduction of N_4; the effect increases with decreasing size of the M cation's ionic radius (increasing ionic potential) and is most strongly pronounced with MgO.
2. Within the series 60 SiO_2–10 B_2O_3–10 Al_2O_3–(20−x) MO−x MgO (M = Ca, Sr, Ba) at any fixed value of x, N_4 decreases linearly with decreasing size (increasing ionic potential) of the alkaline-earth metal.
3. For the all-alkaline-earth oxide series, the successive replacement of MO by MgO leads to a reduction of N_4 as well.

Overall, the universal phenomenon observed here involves a diminution of four-coordinate boron species with increasing average ionic potential ξ of the charge compensating alkaline-earth ion inventory. Figure 4 shows a plot of N_4 versus ξ for all the glasses studied here, illustrating a universal relationship. This result confirms previously discovered findings in borosilicate glasses that the mechanism of anionic compensation in these multiple network former glasses is greatly influenced by the ionic potential of the cation: low ionic potential cations favor four-coordinate boron, whereas high ionic potential cations favor non-bridging oxygen species. The latter could be bound to Si (Si^3 species) or to three-coordinate boron (B^2(III) species). Although a clearly identifiable B^2(III) lineshape component, which would have an asymmetry parameter near 0.5, could not

TABLE 3 ^{11}B NMR interaction parameters extracted from lineshape simulations for the glasses of the system $60SiO_2$–$10B_2O_3$–$10Al_2O_3$–$(20-x)MO$–$xMgO$ ($x = 0, 5, 10$), $60SiO_2$–$10B_2O_3$–$10Al_2O_3$–$10Na_2O$–$10M_{(2)}O$ (M = Ca, Sr, Ba, Na), and $60SiO_2$–$5B_2O_3$–$15Al_2O_3$–10CaO–10MgO. First line: simulation of the spectrum measured at 5.7 T, second line: simulation of the spectrum measured at 14.1 T

		^{11}B					
		B^3(III) – 1/B^3(III)−2				B^4 (IV)	
MgO	CaO	A/% ±2	δ_{iso}/ppm ±0.4	C_Q/MHz ±0.04	η_Q ±0.05	A/% ±2	δ_{iso}/ppm ±0.1
0	20	36/44	15.0/17.6	2.64/2.55	0.28/0.32	20	−1.0
		37/47	14.4/17.0	2.61/2.62	0.28/0.32	16	−0.4
5	15	42/46	14.4/17.6	2.64/2.59	0.2/0.32	12	−1.2
		43/47	14.4/17.0	2.59/2.62	0.28/0.32	10	−0.3
10	10	46/45	14.4/17.6	2.65/2.60	0.28/0.32	9	−1.1
		45/49	14.3/17.0	2.60/2.62	0.28/0.32	6	−0.3

		B^3(III) – 1/B^3(III)−2				B^4 (IV)	
MgO	SrO	A/% ±2	δ_{iso}/ppm ±0.4	C_Q/MHz ±0.04	η_Q ±0.05	A/% ±2	δ_{iso}/ppm ±0.1
0	20	29/41	14.8/17.6	2.65/2.59	0.28/0.32	30	−1.3
		28/41	14.6/17.3	2.59/2.63	0.28/0.32	31	−0.4
5	15	37/46	14.1/17.4	2.65/2.62	0.28/0.32	17	−1.6
		36/48	14.6/17.0	2.60/2.60	0.28/0.32	16	−0.3
10	10	41/49	14.7/17.7	2.64/2.61	0.28/0.32	11	−1.4
		41/51	14.4/17.0	2.60/2.61	0.26/0.32	8	−0.2

		B^3(III) – 1/B^3(III)−2				B^4 (IV)	
MgO	BaO	A/% ±2	δ_{iso}/ppm ±0.4	C_Q/MHz ±0.04	η_Q ±0.05	A/% ±2	δ_{iso}/ppm ±0.1
0	20	23/39	14.8/17.3	2.65/2.58	0.28/0.32	38	−1.6
		23/37	14.9/17.3	2.61/2.61	0.28/0.32	40	−0.5
5	15	35/45	14.1/17.6	2.64/2.61	0.28/0.32	20	−1.4
		34/46	14.7/17.2	2.61/2.64	0.28/0.32	20	−0.4
10	10	37/52	14.3/17.6	2.61/2.59	0.28/0.32	11	−1.1
		39/52	14.6/17.3	2.58/2.65	0.28/0.32	9	−0.2

					^{11}B					
					B^3(III) – 1/B^3(III)−2				B^4 (IV)	
MgO	CaO	SrO	BaO	Na_2O	A/% ±2	δ_{iso}/ppm ±0.4	C_Q/MHz ±0.04	η_Q ±0.05	A/% ±2	δ_{iso}/ppm ±0.1
10				10	89.5[a]	15.3[a]	2.6[a]	0.27[a]	10.5[a]	1.2[a]
	10			10	33/36	15.0/17.9	2.63/2.58	0.28/0.32	31	−1.0
					33/40	14.9/17.5	2.58/2.62	0.28/0.32	27	−0.3
		10		10	26/31	14.9/17.5	2.64/2.58	0.28/0.32	42	−1.0
					23/33	15.0/17.5	2.59/2.58	0.28/0.32	43	−0.4
			10	10	21/31	15.0/17.2	2.64/2.58	0.28/0.32	48	−1.5
					18/32	15.2/17.7	2.63/2.63	0.28/0.32	50	−0.5
				20	42[a]	15.4[a]	2.6[a]	0.24[a]	58[a]	1.6[a]

		^{11}B					
		B^3(III) – 1/B^3(III)−2				B^4 (IV)	
MgO	CaO	A/% ±2	δ_{iso}/ppm ±0.4	C_Q/MHz ±0.04	η_Q ±0.05	A/% ±2	δ_{iso}/ppm ±0.1
10	10	56/40	14.9/17.8	2.61/2.59	0.28/0.32	4	0.1
		55/42	14.6/17.4	2.59/2.65	0.28/0.32	3	−0.2

aFrom Ref. [9] at 5.7 T.

be identified for the latter, small concentrations cannot be ruled out. Finally it is noteworthy that the strongest outlier in Figure 4 is observed for the glass with composition $60SiO_2$–$10B_2O_3$–$10Al_2O_3$–$10MgO$–$10Na_2O$, which shows a substantially lower experimental N_4 value than indicated by the linear relationship. This is the same glass that also does not follow the monotonic correlation of Log(*CR*) versus ξ in Figure 1c. This finding will be discussed further below in connection with a potential partial network former role of Mg in these aluminoborosilicate glasses.

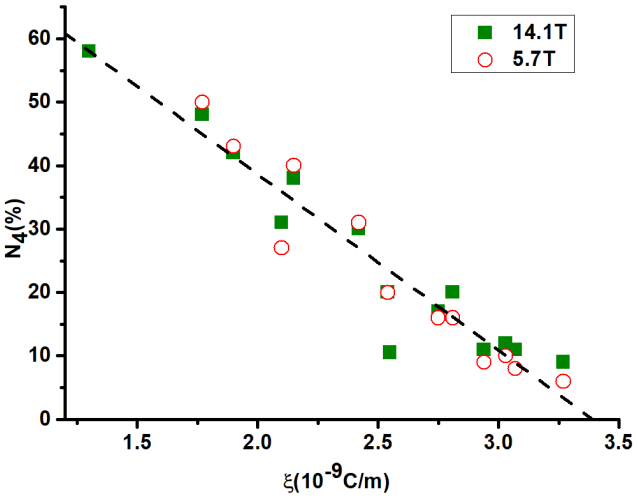

FIGURE 4 Fraction of four-coordinate boron species as a function of average ionic potential in glasses of the system $60SiO_2$–$10B_2O_3$–$10Al_2O_3$–$(20-x)MO$–$xMgO$ ($x = 0, 5, 10$) and $60SiO_2$–$10B_2O_3$–$10Al_2O_3$–$(20-x)Na_2O$–xMO (M = Mg, Ca, Sr, Ba, $x = 0, 5, 10$) [Color figure can be viewed at wileyonlinelibrary.com]

3.3 | ^{29}Si MAS-NMR

Figure 5 shows the ^{29}Si MAS-NMR spectra of the glasses under study. No peak resolution into distinct silicon species can be observed. Rather, the spectra show one broad unresolved resonance line, from which the average isotropic chemical shift can be extracted from the center of gravity (see Table 4). The spectra are likely to be composed of multiple contributions: (1) fully polymerized tetrahedral units, whose resonances are shifted towards higher frequencies compared to SiO_2, owing to the presence of *m* Si–O–Al linkages (Si^4_{mAl} species), (2) analogous Si^4_{mB} species, where the chemical shift effect of a Si–O–B linkage is significantly smaller than that of a Si–O–Al linkage and also depends on the boron coordination number, and (3) Si^3 species connected to non-bridging oxygen atoms. The average ^{29}Si chemical shift of the glass containing 20 mole% Na_2O is found near −93.5 ppm, distinctly higher than the values observed for the analogous alkaline-earth oxide-containing glasses (values between −95 and −98 ppm). Partial substitution of Na by alkaline-earth elements displaces the signal towards lower frequency, by 3–5 ppm, respectively. Again, the low-frequency displacement increases with decreasing size of the alkaline-earth cation, manifesting a monotonic correlation with the average ionic potential of the network modifier as illustrated in Figure 6.

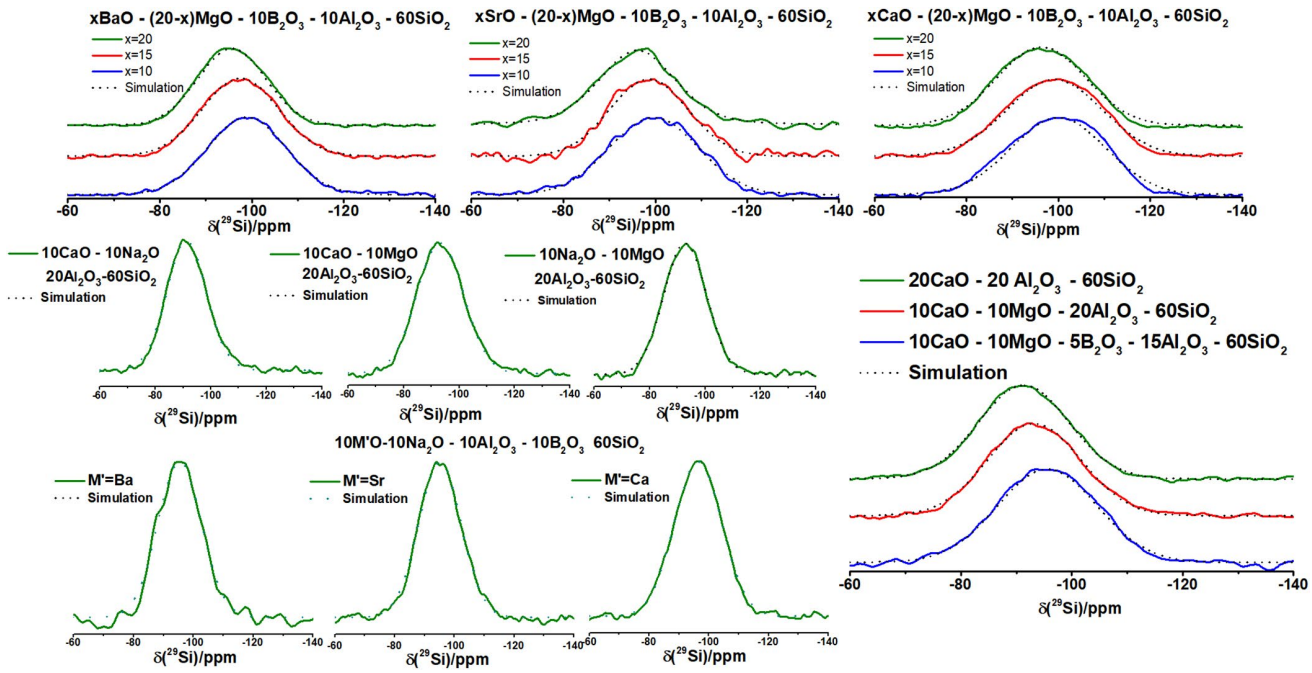

FIGURE 5 ^{29}Si MAS-NMR spectra of $60SiO_2$–$10B_2O_3$–$10Al_2O_3$–$(20-x)MO$–$xMgO$ ($x = 0, 5, 10$) glasses, of $60SiO_2$–$10B_2O_3$–$10Al_2O_3$–$10Na_2O$–$10MO$ (M = Ca, Sr, Ba) glasses, and of three $60SiO_2$–$20Al_2O_3$–$(10M_{(2)}O)$–$xM'O$ glasses with the compositions specified [Color figure can be viewed at wileyonlinelibrary.com]

TABLE 4 Average ^{29}Si chemical shift (center of gravity) and full width at half height of glasses in the system $60SiO_2$–$10B_2O_3$–$10Al_2O_3$–$(20-x)$MO–xMgO (x = 0, 5, 10) and $60SiO_2$–$10B_2O_3$–$10Al_2O_3$–$10Na_2O$–$10M_{(2)}O$ (M = Ca, Sr, Ba, Na). Additional results on some aluminosilicate glasses are included as well

					^{29}Si	
MgO	CaO	SrO	BaO	Na_2O	δ_{iso}/ppm (±0.5)	FWHM/ppm (±0.5)
0	20				−98.3	22.8
5	15				−99.2	24.5
10	10				−100.0	24.3
0		20			−97.0	20.0
5		15			−98.6	20.1
10		10			−99.7	23.0
0			20		−95.7	17.6
5			15		−97.5	19.7
10			10		−98.9	20.2
10				10	−98.6[a]	17.4[a]
	10			10	−96.4	18.8
		10		10	−95.4	17.1
			10	10	−95.2	16.8
				20	−93.5[a]	18.0[a]
Boroaluminosilicate glass: $5B_2O_3$–$15Al_2O_3$–$60SiO_2$–5MO–15M'O						
					^{29}Si	
MgO	CaO	SrO	BaO	Na_2O	δ_{iso}/ppm (±0.5)	FWHM/ppm (±0.5)
5	15				−95.6	21.1
Aluminosilicate glasses: $20Al_2O_3$–$60SiO_2$–$10M_{(2)}O$–10M'O						
					^{29}Si	
MgO	CaO	SrO	BaO	Na_2O	δ_{iso}/ppm (±0.5)	FWHM/ppm (±0.5)
	10			10	−91.2	17.0
	20				−91.3	19.1
10	10				−93.2	19.9

[a]From Ref. [9].

Overall, these results suggest that MgO (and other high ion potential modifiers) has the effect of decreasing the Si–O–Al connectivity in these glasses; we view this to be the dominant effect upon the average chemical shift in the present series of glasses. Our interpretation is supported by ^{29}Si{^{27}Al} REAPDOR comparisons between a sodium and a magnesium aluminosilicate glass with the 20-20-60 composition, suggesting a reduced extent of Si–O–Al connectivity in the Mg-containing glass.[9] A further contribution towards the systematic displacements of the average ^{29}Si chemical shift towards lower frequency upon Na → alkaline-earth substitution may arise from a diminished contribution of Si–O–B(IV) linkages, as the fraction of B(IV) units is decreased with increasing average ion potential. However, as the four-coordinated boron species have low overall concentrations their impact on the glass structure is small.

Finally, the ^{29}Si chemical shift trends do not support an increase in the concentration of Si^3 units as a consequence of charge balancing demands which must be met when Si–O–Al linking and/or B(IV) contents are diminished in Mg-containing glasses. An increase in Si^3 units would contribute to higher-frequency shifts of the ^{29}Si signals, which is opposite to what is observed experimentally. As discussed further below, this may be taken as evidence for Mg partially adopting a network former role in these glasses.

3.4 | ^{27}Al MAS-NMR

Figure 7 shows the ^{27}Al MAS-NMR spectra of all the glasses, measured at 14.1 T. Only the central $m = ½ \leftrightarrow m = -½$ Zeeman transition of the ^{27}Al nuclear spins ($I = 5/2$) is observed. All the spectra show the typical asymmetric lineshape at isotropic chemical shifts between 57 and 63 ppm, which could be satisfactorily fitted by a distribution of quadrupolar coupling constants, based on the Czjzek model.[32] Table 5 summarizes the results. Al occurs almost exclusively in the four-coordinate state (Al(IV) units, which are generally assumed to be linked to other network forming units via four bridging oxygen atoms, i.e. occurring as anionic $AlO_{4/2}^-$ (Al^4) units. Overall, this result stands in good agreement with the findings in the literature on charge-balanced sodium aluminosilicate glasses:[28,36–38] for the chosen compositions, all the anionic $AlO_{4/2}^-$ sites can be charge balanced by alkaline or alkaline-earth ions, producing a highly polymerized tetrahedral network. Within each $(M_{(2)}O)_{20-x}(MgO)_x$ series, however, there is a systematic trend of the linewidth to increase, indicating an increase in the average ^{27}Al nuclear electric quadrupolar coupling constant $\langle C_Q \rangle$ with increasing MgO content x, in good agreement with previous findings on related boro- and aluminosilicate glasses.[9] This result indicates that the interaction of Al^4 units with Mg^{2+} tends to increase the local distortions of the oxygen environment. Evidently charge neutralization of the anionic Al^4 species by Mg^{2+} produces a larger degree of local distortion at the aluminum sites than charge neutralization by Na^+. Figure 8a indicates that, when glasses with different alkaline-earth inventories are examined, this effect can again be correlated with its average ionic potential. The extent of scatter is larger in this case, possibly because the random error of the $\langle C_Q \rangle$ determination is larger than for the average ^{29}Si isotropic chemical shift or the ^{11}B-N_4 value. Two mechanisms promoted by the high-field strength cation Mg^{2+} can be envisioned leading to the formation of Al species not observed in alkali aluminosilicate glasses: Al species involved in either Al^4–O–Al^4 linkages or four-coordinate Al species carrying non-bridging oxygen atoms (Al^3(IV) units).[39,40] The structural relevance of such seemingly energetically unfavorable units was recently demonstrated by ^{17}O{^{27}Al} dipolar recoupling NMR experiments.[40] While in alkali aluminosilicate glasses such units are suppressed because of

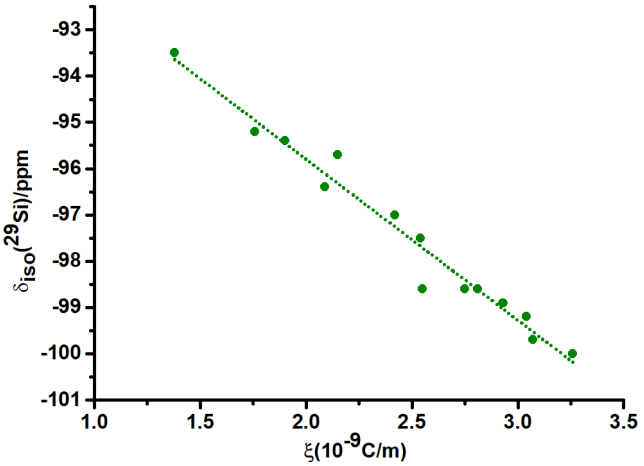

FIGURE 6 Correlation of average ^{29}Si chemical shifts of $60SiO_2$–$10B_2O_3$–$10Al_2O_3$–$(20-x)$MO–xMgO ($x = 0$, 5, 10) glasses, and of $60SiO_2$–$10B_2O_3$–$10Al_2O_3$–$10Na_2O$–$10M_{(2)}O$ (M = Na, Ca, Sr, Ba) glasses with the average ionic potentials [Color figure can be viewed at wileyonlinelibrary.com]

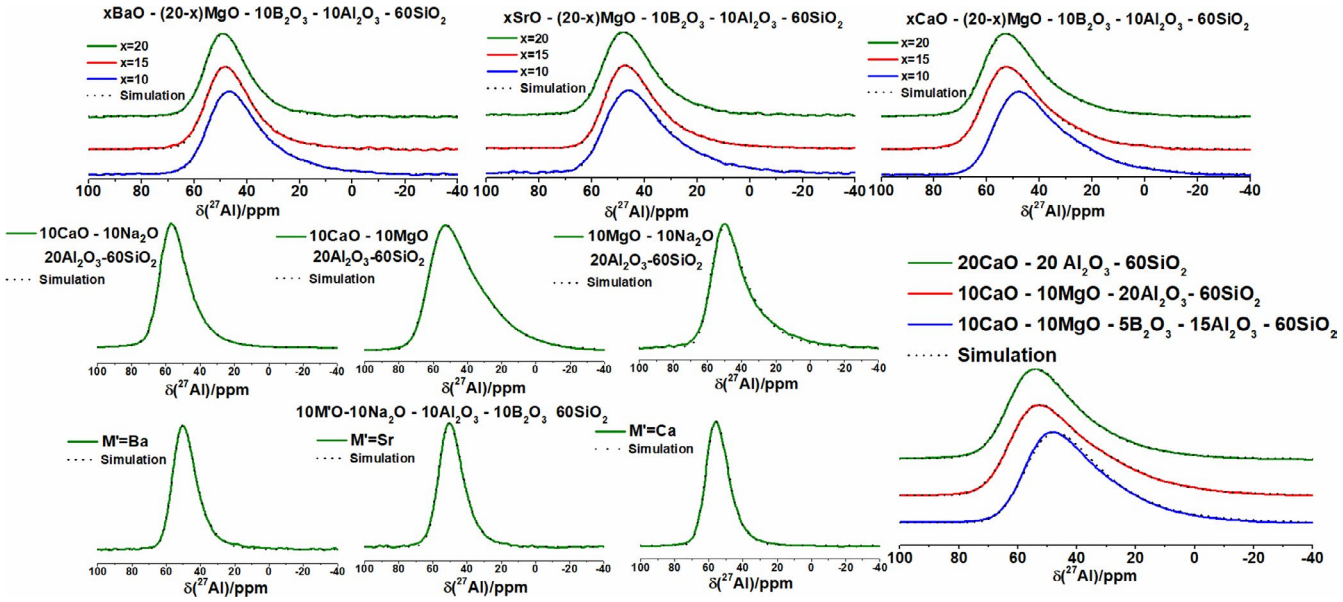

FIGURE 7 ^{27}Al MAS-NMR spectra of glasses in the system $60SiO_2$–$10B_2O_3$–$10Al_2O_3$–$(20-x)$MO–xMgO ($x = 0$, 5, 10), $60SiO_2$–$10B_2O_3$–$10Al_2O_3$–$10Na_2O$–10MO (M = Ca, Sr, Ba), and $60SiO_2$–$20Al_2O_3$–$10M_{(2)}O$–10M'O (M = Na, Ca, M' = Ca, Mg) [Color figure can be viewed at wileyonlinelibrary.com]

TABLE 5 ^{27}Al isotropic chemical shifts and average nuclear electric quadrupolar coupling constants $\langle C_Q \rangle$ of glasses in the system $60SiO_2$–$10B_2O_3$–$10Al_2O_3$–$(20-x)$MO–xMgO and $60SiO_2$–$10B_2O_3$–$10Al_2O_3$–$10Na_2O$–$10M_{(2)}O$

					^{27}Al	
MgO	CaO	SrO	BaO	Na_2O	δ_{iso}/ppm (±1)	$\langle C_Q \rangle$ / MHz (±0.1)
0	20				61	7.1
5	15				61	7.5
10	10				58	8.1
0		20			58	6.3
5		15			58	6.8
10		10			58	7.5
0			20		58	5.6
5			15		57	6.0
10			10		57	6.9
10				10	60[a]	4.5[a]
	10			10	61	4.8
		10		10	58	5.2
			10	10	58	5.3
				20[a]	61	4.2[a]
Boroaluminosilicates: $5B_2O_3$–$15Al_2O_3$–$60SiO_2$–5MO–15M'O						
					^{27}Al	
MgO	CaO	SrO	BaO	Na_2O	δ_{iso}/ppm (±1)	$\langle C_Q \rangle$ / MHz (±0.1)
5	15				60	8.2
Aluminosilicates: $20Al_2O_3$–$60SiO_2$–10MO–$10M_{(2)}$'O						
					^{27}Al	
MgO	CaO	SrO	BaO	Na_2O	δ_{iso}/ppm (±0.5)	$\langle C_Q \rangle$ / MHz (±0.1)
	10			10	63	5.8
	20				63	7.5
10	10				64	8.6

[a]From Ref. [9].

the unfavorable Coulombic repulsion of two negative charges in close proximity they might be stabilized by doubly charged cations with high ionic potential such as Mg^{2+}.

The asymmetric lineshape, characterized by the systematic sloping of the spectra towards lower frequencies, which is a consequence of the distribution of electric field gradients, nevertheless raises the question whether there may be hidden contributions from five- and six-coordinated aluminum. To probe this possibility we conducted both ^{27}Al satellite transition (SATRAS)[41] and ^{27}Al triple quantum MAS-NMR studies.[42] Both experiments enhance the spectroscopic resolution by minimizing anisotropic broadening of the ^{27}Al MAS-NMR spectra due to second-order quadrupolar effects. Exemplary spectra are shown in Figures S2 and S3 of the Supporting Materials Section. However, in none of the glasses of this study, any five- or six-coordinate ^{27}Al could be identified, neither in the SATRAS nor in the TQMAS-NMR data. These results indicate that the replacement of Na_2O (or any of the alkaline-earth oxides) by MgO does not produce higher-coordinated Al species in significant amounts in this series of glasses. As previously shown the only related glass revealing significant concentrations of higher-coordinate aluminum in both the TQMAS- and the SATRAS data is the purely MgO-containing sample $60SiO_2$–$20Al_2O_3$–20MgO.[9] In that sample, the amount of higher-coordinated aluminum is estimated at 16 ± 2% Al(V) and 2 ± 2% Al(VI). Minor amounts of Al(V) have also been detected in $60SiO_2$–$20Al_2O_3$–10MgO–$10Na_2O$ glass.[9] Overall, the trends observed in this study are in excellent agreement with previous results obtained on other aluminoborosilicate glasses.[9–23]

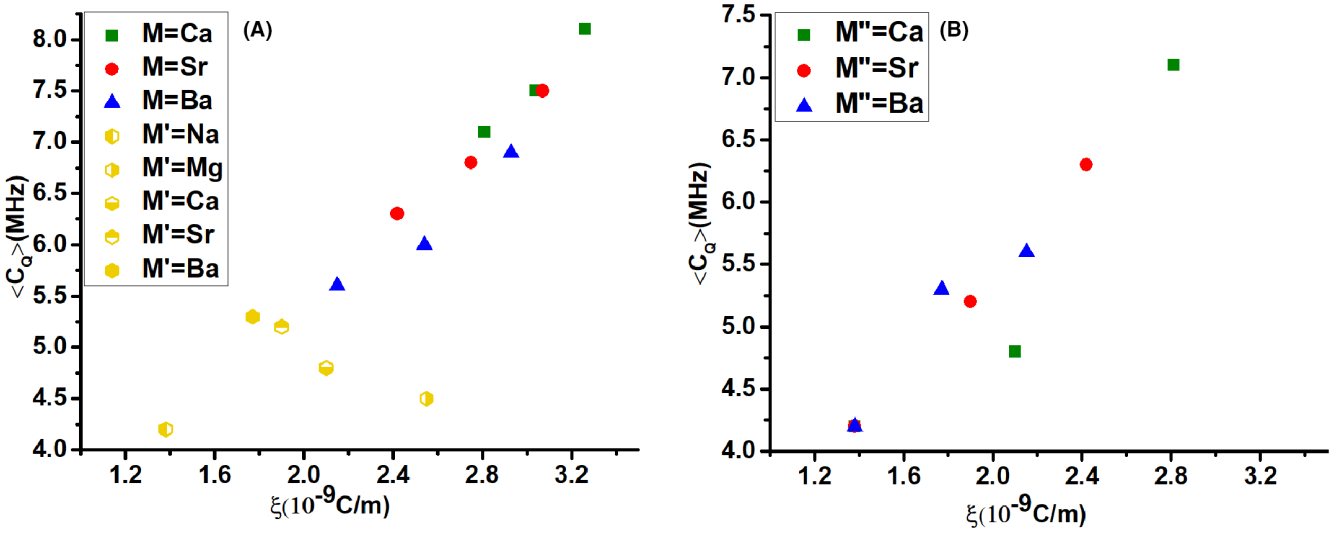

FIGURE 8 Correlation of the average ^{27}Al quadrupolar coupling constants $\langle C_Q \rangle$ with the average ionic potential for glasses in: (a) the systems $60SiO_2$–$10B_2O_3$–$10Al_2O_3$–$(20-x)$MO–xMgO (M = Ca, Sr, Ba) and $60SiO_2$–$10B_2O_3$–$10Al_2O_3$–$10Na_2O$–$10M_{(2)}$'O (M' = Na, Mg, Ca, Sr, Ba), and (b) the system $60SiO_2$–$10B_2O_3$–$10Al_2O_3$–$(20-x)Na_2O$–xM"O (M" = Ca,Sr,Ba) [Color figure can be viewed at wileyonlinelibrary.com]

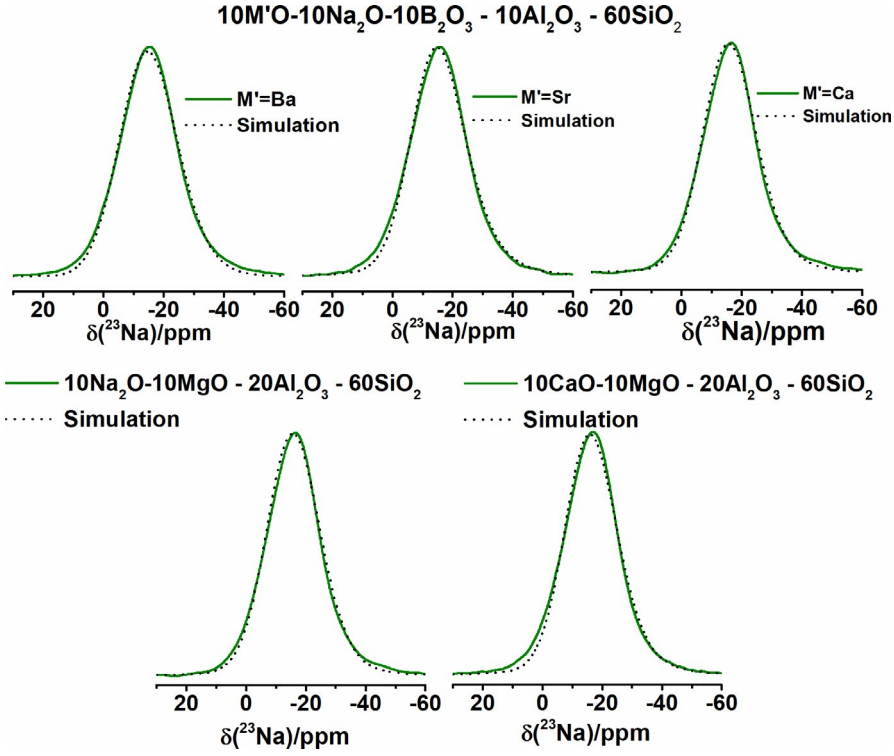

FIGURE 9 ^{23}Na MAS-NMR spectra of glasses with composition $60SiO_2$–$10B_2O_3$–$10Al_2O_3$–$10Na_2O$–10MO and $60SiO_2$–$20Al_2O_3$–$10Na_2O$–10MO [Color figure can be viewed at wileyonlinelibrary.com]

Figure 8a shows the relationship between $\langle C_Q \rangle$ (^{27}Al) and ξ of all the glasses of this study. Except for the Na-Ca and Na-Mg glasses (yellow symbols), there seems to be a good correlation. The subset series of the glasses in which Na_2O is substituted for MO (M = Ca, Sr and Ba) were extracted and the linear relationship is re-verified in Figure 8b, with a minor deviation observed for the Na-Ca glass). Only the data point referring to the Na-Mg glass in Figure 8a does not fit this correlation.

3.5 | ^{23}Na MAS-NMR

Figure 9 summarizes the ^{23}Na MAS-NMR spectra of all the Na-containing glasses (central $m = ½ \leftrightarrow m = -½$ transitions). Similarly, as for ^{27}Al, the asymmetrically broadened lineshapes suggest a high degree of disorder in the local environment around Na. This is supported by the excellent agreement with the one-component Czjzek model deconvolutions

TABLE 6 ^{23}Na MAS-NMR parameter of the Na-containing glasses

Boroaluminosilicates: $10B_2O_3$–$10Al_2O_3$–$60SiO_2$–$10Na_2O$–$10M_{(2)}$'O						
					^{23}Na	
MgO	CaO	SrO	BaO	Na_2O	δ_{iso}/ppm ±0.5	$\langle C_Q \rangle$ / MHz (±0.1)
				20	−8.6[a]	2.5[a]
10				10	−12.0[a]	2.0[a]
	10			10	−11.4	2.1
		10		10	−9.6	2.4
			10	10	−9.5	2.2

Aluminosilicates: $20Al_2O_3$–$60SiO_2$–$10Na_2O$–M'O				
			^{23}Na	
MgO	CaO	Na_2O	δ_{iso}/ppm ±0.5	$\langle C_Q \rangle$ / MHz (±0.1)
10		10	−11.4	2.1
	10	10	−11.7	2.0

[a]From Ref. [9].

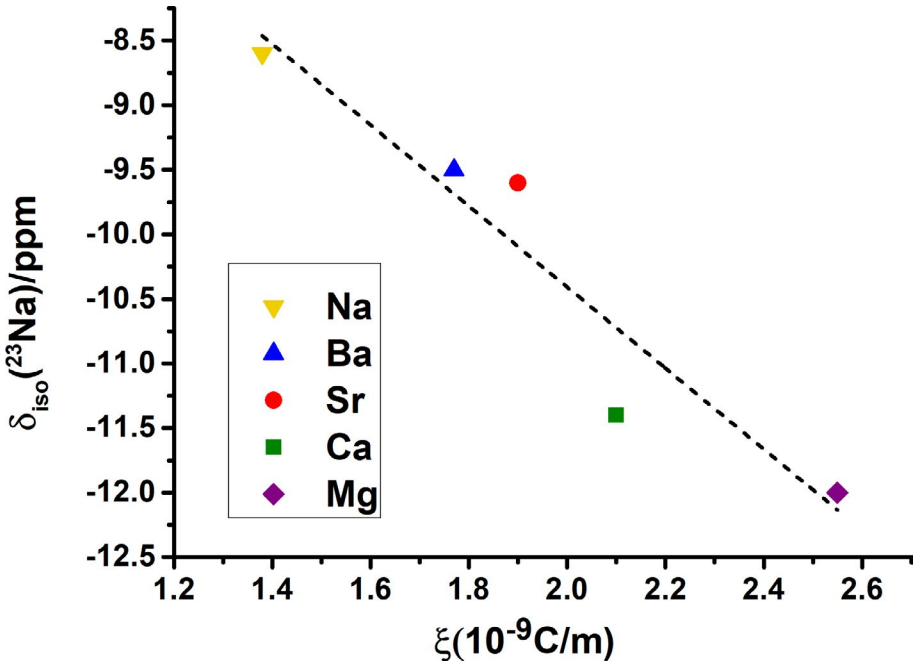

FIGURE 10 Correlation of ^{23}Na isotropic chemical shifts δ_{iso}^{cs} with average ionic potential in glasses with composition $60SiO_2$–$10B_2O_3$–$10Al_2O_3$–$10Na_2O$–10MO [Color figure can be viewed at wileyonlinelibrary.com]

(Table 6). The limited amount of data available indicate a trend of the ^{23}Na isotropic chemical shifts to become more negative with increasing ionic potential of the second cation present (see Figure 9, bottom). The interpretation of such subtle chemical shift trends is difficult. In general, ^{23}Na chemical shifts reflect both the coordination number and the covalence of the Na–O bonding,[43,44] which, in turn, is affected by the other elements (network formers and modifiers) with which these oxygen atoms are being shared. The shift of the ^{23}Na signals in the mixed Na-Mg and other alkaline-earth glasses towards lower frequencies is also observed in mixed Na-Li borate glasses and indicates that the Na–O bonds are less covalent (and the sites are possibly somewhat expanded) in these glasses than in the corresponding single-alkali glasses.[44]

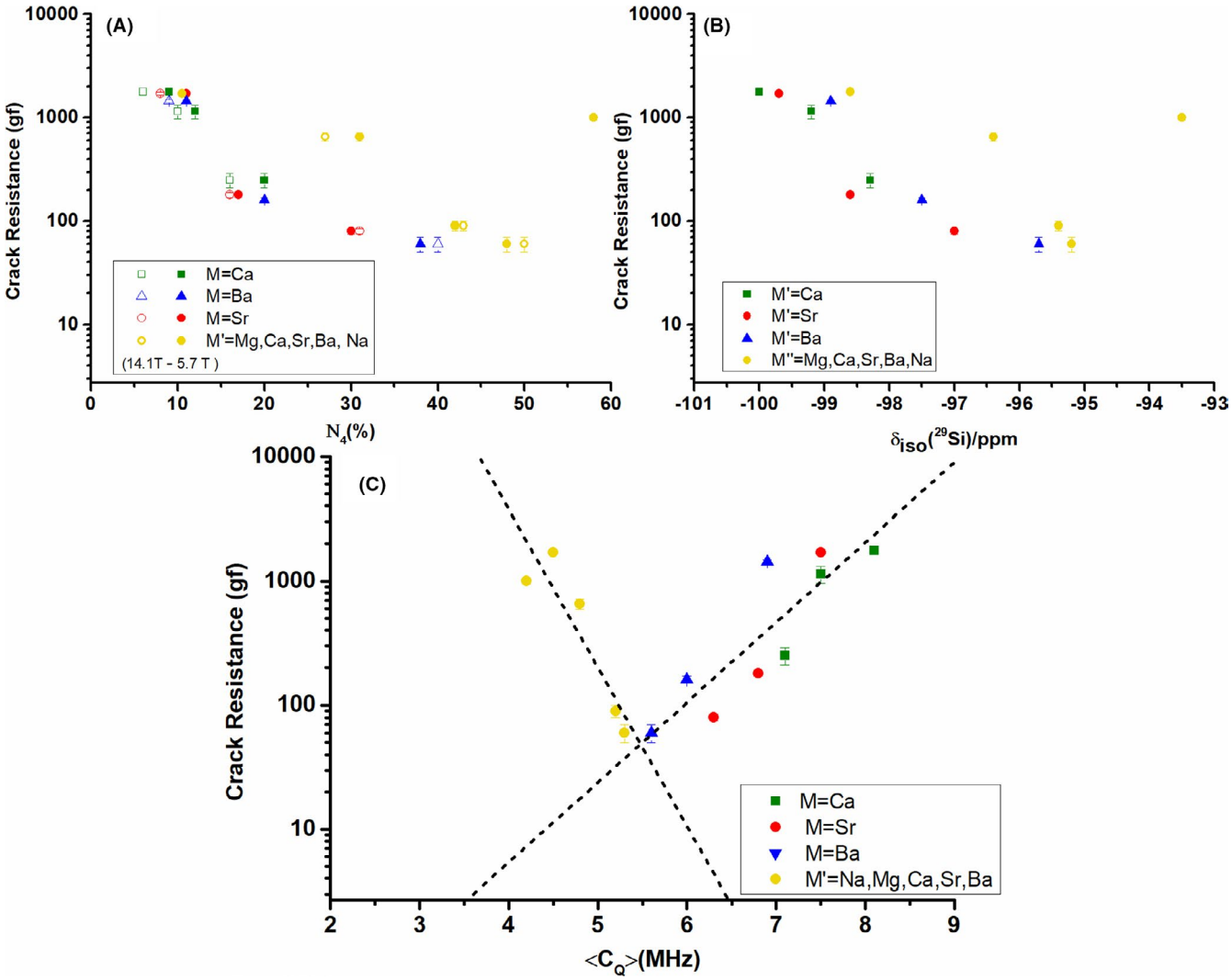

FIGURE 11 Correlation of Crack Resistance with (A) the fraction of four-coordinate boron species, (B) the average ^{29}Si chemical shift, and (C) the average ^{27}Al quadrupolar coupling constants for glasses in the systems $60SiO_2$–$10B_2O_3$–$10Al_2O_3$–$(20–x)MO$–$xMgO$ (M = Ca, Sr, Ba) and $60SiO_2$–$10B_2O_3$–$10Al_2O_3$–$10Na_2O$–10M'O (M' = Na, Mg, Ca, Sr, Ba) [Color figure can be viewed at wileyonlinelibrary.com]

4 | DISCUSSION

4.1 | Correlation of structural and functional properties

Figure 1a,b show that log(*CR*) is linearly correlated with the average ionic potential as calculated from the cation inventory of these glasses, in both mixed alkaline-earth aluminoborosilicate glasses and in mixed Na_2O-alkaline-earth aluminoborosilicate glasses with fixed Na_2O/alkaline-earth oxide ratio. Simultaneously, Figures 4, 6, 8, and 10 reveal that the chief multinuclear NMR observables for the network former species, namely $N_4(^{11}B)$, $\delta_{iso}(^{29}Si)$, and $<C_Q>$ (^{27}Al), show monotonic uniform linear dependences on the average ionic potential. As Figure 11 illustrates, then, all these NMR observables show linear correlations with log(*CR*), leading to the conclusion that enhanced crack initiation resistances are correlated with reduced B(IV) content, fewer Al–O–Si linkages, and more distorted Al(IV) local environments. The effect of Mg on the crack resistance thus can be understood in terms of these structural parameters, which in turn arise as a consequence of the high ionic potential of Mg^{2+}. This effect may be due to the increased presence of either Al^4–O–Al^4 linkages or Al^3(IV) units (four-coordinate Al attached to one non-bridging oxygen) in the Mg-containing glasses.[39,40] The structural relevance of such seemingly energetically unfavorable units was recently demonstrated by $^{17}O\{^{27}Al\}$ dipolar recoupling experiments.[40] While in alkali aluminosilicate glasses such units are suppressed because of the unfavorable Coulombic repulsion of two negative charges in close proximity they might be stabilized by doubly charged cations with high ionic potential such as Mg^{2+}.

In glasses with variable Na_2O/alkaline-earth oxide ratios (Figure 1c) the correlation between log(*CR*) and structural parameters is less straightforward. This behavior may be related to the fact, that the overall cation concentration in the latter system is not constant, but increases linearly

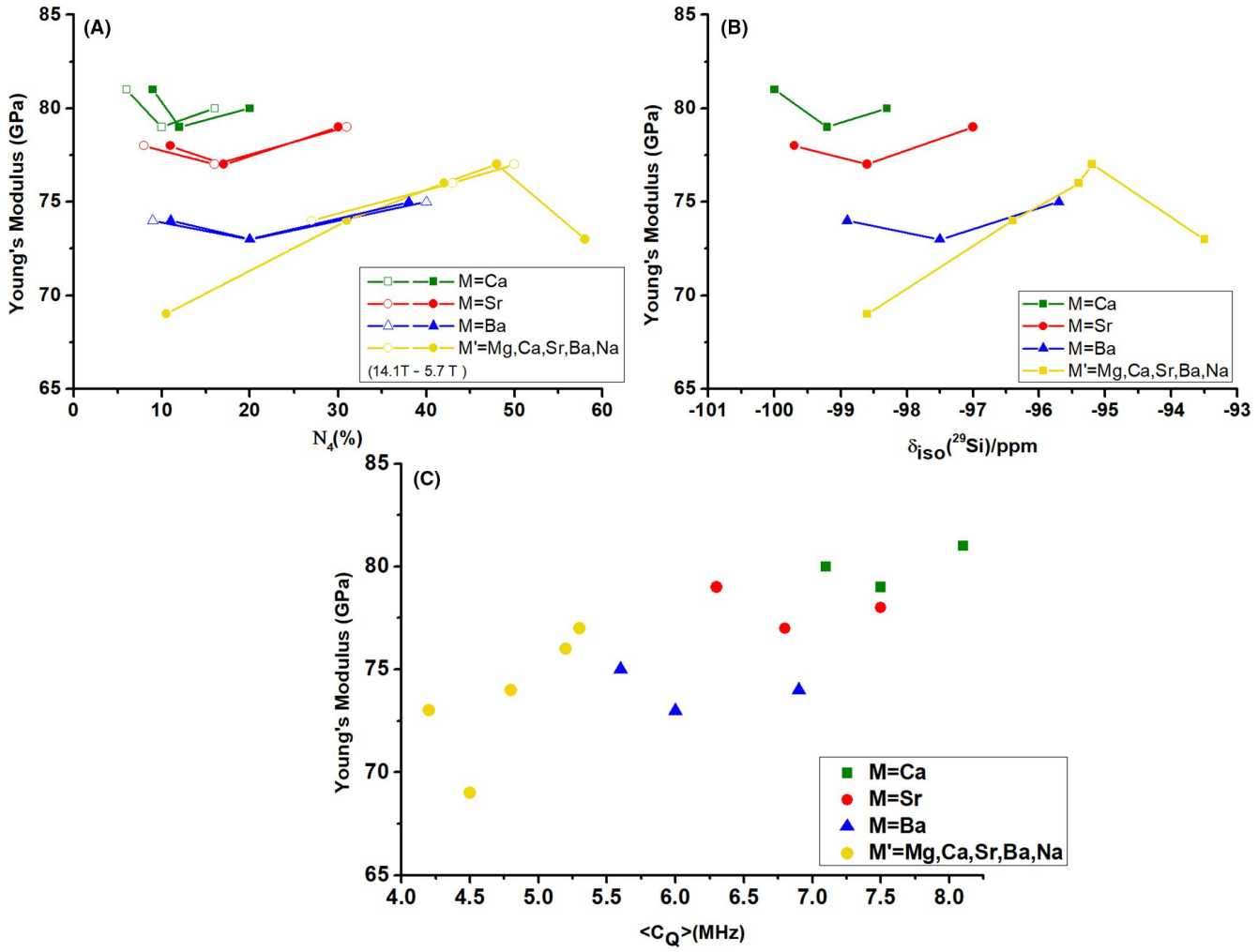

FIGURE 12 Correlation of Young's Modulus with (A) the fraction of four-coordinate boron species, (B) the average ionic potential and (C) the average ^{27}Al quadrupolar coupling constants for glasses in the systems $60SiO_2$–$10B_2O_3$–$10Al_2O_3$–$(20-x)$MO–xMgO (M = Ca, Sr, Ba) and $60SiO_2$–$10B_2O_3$–$10Al_2O_3$–$10Na_2O$–10M'O (M' = Na, Mg,Ca, Sr, Ba) [Color figure can be viewed at wileyonlinelibrary.com]

with increasing Na_2O content. The necessity of the structure to accommodate increasing amounts of Na^+ ions along this series can be expected to have additional structural impact that cannot be described by the cation's ability to polarize its local environment. As evident from Figure 11, the glasses with cation contents of 20% Na_2O, 10%Na_2O–10%MgO and 10%Na_2O–10%CaO do not follow the correlations exhibited by the other glasses. Notably, these are the same glasses for which the crack resistances deviate from values predicted from the trends based on average ionic potential in Figure 1c. In connection with Figure 8a, we suspect that this behavior may be related to the state of the aluminum species: experimental $<C_Q>$ values for these glasses are found lower than expected from the general trend of the ξ values. We suspect that these glasses may contain small amounts of Al(V) or Al(VI) units that went undetected by ^{27}Al MAS- and TQMAS-NMR but still influence the macroscopic physical properties of these glasses. In addition (as discussed further below), the results obtained on the $10Na_2O$–10MgO glass in particular may suggest that Mg partially adopts a network former role.

Figure 12 explores analogous correlations between Young's modulus E and the three aforementioned structural parameters. E follows the same trends with $<C_Q>$(^{27}Al) and δ_{iso}(^{29}Si) as log(CR), suggesting that the formation of highly distorted Al(IV) environments (and the associated decrease in Si–O–Al connectivities) enhances both parameters in parallel. In contrast, the correlation of E with N_4 (^{11}B) is exactly the opposite of the one observed for the crack initiation resistance. Thus, if the physical parameters are dominated by the boron coordination (as they are in borosilicate glasses), high crack resistance would come at the price of low modulus and vice versa. In aluminoborosilicate glasses, however, the physical properties can be additionally influenced by the details of the aluminum coordination, which is—again—modified by the ion potential of the alkaline-earth cation. In this case the more highly distorted Al(IV) environments promoted by the high-ξ cations (in particular Mg^{2+}) have the effect

of increasing *CR* and *E* in parallel. The special role of Mg-containing glasses as compared to the other alkaline-earth species can thus be explained as follows: crack resistance is strongly enhanced because the high ion potential disfavors the formation of B(IV) units and promotes more strongly distorted Al(IV) environments. However, the enhanced *CR* does not come at the price of a lowered *E* because the negative effect of the N_4 reduction on *E* is counterbalanced by the positive effect exerted on this parameter by the highly distorted Al environments.

Again, we may note that the three glasses with cation contents of $20Na_2O$, $10Na_2O$–10MgO and $10Na_2O$–10CaO show different behavior and do not follow the correlations exhibited by the other glasses. In alkaline-earth aluminosilicate glasses this phenomenon can be understood on the basis of five- and six-coordinated aluminum which is only present in considerable amounts in the Mg-containing glasses.[9] In the present aluminoborosilicate glasses, however, no higher-coordinated Al could be detected, even though we cannot rule out the possibility that low concentrations of such species are present.

4.2 | The special role of Mg in aluminoborosilicate glasses

Finally, the joint interpretation of Figures 4, 6 and 8 warrants a discussion of the special role of Mg in aluminoborosilicate glasses: Evidently, the low anionic B(IV) concentrations of Mg-containing glasses must imply the existence of an alternative charge balancing scheme. Regarding the generation of more non-bridging oxygen species, our ^{11}B MAS-NMR data do not provide clear evidence for higher concentrations of B^2(III) units in the Mg-containing glasses. Such B^2(III) units would produce a lineshape contribution from three-coordinate boron species with electric field gradient asymmetry parameters near 0.5, for which we have no clear evidence. Furthermore, the ^{29}Si MAS-NMR spectra provide no evidence for an enhanced Si^3 contribution; rather the opposite chemical shift effect (towards lower frequencies) is observed in Mg-containing glasses. A structural mechanism that could explain both, the low-frequency shift of the ^{29}Si NMR signal (reflecting less Si–O–Al linking) and the reduced N_4 values, is based on the idea that Mg^{2+}, unlike the other alkaline-earth metal ions, may partly adopt a network former role, being integrated in the network structure in the form of $MgO_{4/2}^{2-}$ species, ie, Mg^4 units linking to the other network formers via four bridging oxygen atoms. This idea has been previously proposed for both silicate[45] and borate glasses.[46] In the present glass series, this mechanism should be considered for the glass with composition $60SiO_2$–$10B_2O_3$–$10Al_2O_3$–10MgO–$10Na_2O$, which shows a substantially lower experimental N_4 value than indicated by the linear relationship. This is the same glass that also does not follow the monotonic correlation of Log(*CR*) versus ξ in Figure 1c. Based on this result, one could envision that a distinct contribution to the crack initiation resistance results if Mg is partially found in a network former role.

We wish to emphasize, however, that the suggestion of Mg partially adopting a network former role is based solely on indirect evidence. ^{25}Mg NMR studies might possibly shed light on this issue, however, the NMR properties of this isotope are not very favorable, being characterized by a low natural abundance (10%), a small magnetic moment and a large nuclear electric quadrupole moment. Previous ^{25}Mg NMR work in glasses has revealed that the chemical shift range in oxide glasses is rather narrow.[47–49] To overcome these drawbacks NMR studies on isotopically enriched samples complemented by isotope-selective neutron diffraction studies may be helpful. Additional evidence may come from ^{17}O NMR work, if the oxygen atoms involved in covalent Si^4–O–Mg^4 linking and/or "free oxygen" species associated with Mg-rich domains show a distinct spectroscopic signature.

5 | CONCLUSIONS

The structure of alkali and alkaline-earth aluminoborosilicate glasses with compositions $60SiO_2$–$10B_2O_3$–$10Al_2O_3$–$(20-x)$ MO–xMgO (x = 0, 5, 10) and $60SiO_2$–$10B_2O_3$–$10Al_2O_3$–$10Na_2O$–10MO (M = Mg, Ca, Sr, Ba) is significantly affected by the ionic potentials of the participating alkaline and alkaline-earth ions. Cations with high ionic potential tend to (1) decrease the fraction of four-coordinate boron, (2) diminish the extent of Si–O–Al linking, and (3) increase the level of structural distortion for four-coordinate aluminum species in the network. Monotonic linear trends in ^{11}B-N_4, average ^{29}Si chemical shifts, and average ^{27}Al nuclear electric quadrupolar coupling constants are observed as a function of average ion potential of the cation composition. For the mixed alkaline-earth-containing glasses trends in the enhanced crack initiation resistance can be understood in terms of the above structural variations associated with the increased average ion potential. The incorporation of MgO into these aluminoborosilicate glasses in particular allows enhancing the crack initiation resistance without the trade-off of a reduction in Young's modulus. While the data can be consistently interpreted in terms of Mg adopting a network former role, particularly in the mixed Na_2O-MgO glass, they do not provide direct experimental evidence for this hypothesis. For addressing this issue in further detail, systematic composition-dependent ^{25}Mg and ^{17}O NMR work on isotopically enriched materials, along with neutron diffraction work accompanied by isotopic substitution will be required. These studies are currently under consideration in our laboratory. Altogether the presence of MgO in aluminoborosilicate glasses helps overcome the trade-off issue

between high crack resistance and high elasticity modulus present in borosilicate glasses, thereby offering additional opportunities for the design of glasses that are both very rigid and very crack resistant.

ACKNOWLEDGEMENTS

Support by Nippon Electric Glass Co., Ltd. is gratefully acknowledged. The NMR equipment used for the measurements was acquired with FAPESP funding, CEPID project 2013-07793-6.

CONFLICT OF INTEREST

There are no conflicting financial interests.

ORCID

Millena Logrado https://orcid.org/0000-0002-1655-0061
Hellmut Eckert https://orcid.org/0000-0002-6536-0117

REFERENCES

1. Wondraczek L, Mauro JC, Eckert J, Kühn U, Horbach J, Deubener J, et al. Towards ultrastrong glasses. Adv Mater. 2011;23:4578–86.
2. Sehgal J, Ito S. A new low-brittleness glass in the soda-lime-silica glass family. J Am Ceram Soc. 1998;81:2485–8.
3. Limbach R, Winterstein-Beckmann A, Dellith J, Möncke D, Wondraczek L. Plasticity, crack initiation, and defect resistance in alkali borosilicate glasses. From normal to anomalous behavior. J Non-Cryst Solids. 2015;417–418:15–27.
4. Kato Y, Yamazaki H, Kubo Y, Yoshida S, Matsuoka J, Akai T. Effect of B_2O_3 content on crack initiation under Vickers indentation test. J Ceram Soc Jpn. 2010;118:792–8.
5. Bechgaard TK, Goel A, Youngman RE, Mauro JC, Rzoska SJ, Bockowski M, et al. Structure and mechanical properties of compressed sodium aluminosilicate glasses: role of non-bridging oxygens. J Non-Cryst Solids. 2016;441:49–57.
6. Rosales-Sosa GA, Masuno A, Higo Y, Inoue H. Crack-resistant Al_2O_3-SiO_2 glasses. Sci Rep. 2016;6:23620.
7. Januchta K, Youngman RE, Goel A, Bauchy M, Rzoska SJ, Bockowsky M, et al. Structural origin of high crack resistance in sodium aluminoborate glasses. J Non-Cryst Solids. 2017;460:54–65.
8. Fredriksen KF, Januchta K, Mascaraque N, Youngman RE, Bauchy M, Rzsoska SJ, et al. Structural compromise between high hardness and crack resistance in aluminoborate glasses. J Phys Chem B. 2018;122:6282–95.
9. Bradtmüller H, Uesbeck T, Eckert H, Murata T, Nakane S, Yamazaki H. Structural origins of crack-resistance in magnesium aluminoborosilicate glasses studied by solid state NMR. J Phys Chem C. 2019;123:14941–54.
10. Wu J, Stebbins JF. Quench rate and temperature effects on boron coordination in alminoborosilicate melts. J Non-Cryst Solids. 2010;356:2097–108.
11. Wu J, Stebbins JF. Effects of Cation field strength on the structure of aluminoborosilicate glasses: high-resolution ^{11}B, ^{27}Al, and ^{23}Na MAS-NMR. J Non-Cryst Solids. 2009;355:556–62.
12. Zhang XH, Yue YL, Wu HT. Effect of cation field strength on structure and properties of boroaluminosilicate glasses. Mater Res Innov. 2013;17:212–7.
13. Zhang X, Yue Y, Wu H. Effects of MgO/CaO on the structural, thermal and dielectric properties of aluminoborosilicate glasses. J Mater Sci: Mater Electron. 2013;24:2755–60.
14. Lee SK, Kim HI, Kim EJ, Mun KY, Ryu S. Extent of disorder in magnesium aluminosilicate glasses, insights from ^{27}Al and ^{17}O NMR. J Phys Chem C. 2016;120:737–49.
15. Morin EI, Stebbins JF. Multinuclear NMR investigation of temperature effects on structural reactions involving non-bridging oxygens in multicomponent oxide glasses. J Non-Cryst Solids. 2017;471:179–86.
16. Morin EI, Wu J, Stebbins JF. Modifier cation (Ba, Ca, La, Y) field strength effects on aluminum and boron coordination in aluminoborosilicate glasses: the roles of fictive temperature and boron content. Appl Phys A. 2014;116:479–90.
17. Yamashita H, Yoshino H, Nagata K, Inoue H, Nakajin T, Maekawa T. Nuclear magnetic resonance studies of of alkaline earth phosphosilicate and aluminoborosilicate glasses. J Non-Cryst Solids. 2000;270:48–59.
18. Zheng QJ, Youngman RJ, Hogue CL, Mauro JC, Potuzak M, Smedskjaer MM, et al. Structure of boroaluminosilicate glasses. Impact of the $[Al_2O_3]/[SiO_2]$ ratio on the structural role of sodium. Phys Rev B. 2012;86:054203.
19. Backhouse DJ, Corkhill CL, Hyatt NC, Hand RJ. Investigation of the role of Mg and Ca in the structure and durability of aluminoborosilicate glass. J Non-Cryst Solids. 2019;512:41–52.
20. Jolivet V, Josse L, Rivoal M, Paris M, Morizet Y, Carole L, et al. Quantification of boron in aluminoborosilicate glasses using Raman and ^{11}B NMR. J Non-Cryst Solids. 2019;511:50–61.
21. Yamashita H, Inoue K, Nakajin T, Inoue H, Maekawa T. Nuclear magnetic resonance studies of 0.139MO (or M'_2O) $0.673SiO_2$ $(0.188\text{-}x)Al_2O_3.xB_2O_3$ (M = Ca, Mg, Ca, Sr, and Ba, M' = Na and K) glasses. J Non-Cryst Solids. 2003;331:128–36.
22. Huang S, Li S, Wu F, Yue Y. Effect of B_2O_3 on structure and properties of CaO-MgO-B_2O_3-Al_2O_3-SiO_2 glasses. J Inorg Organmet Polym. 2015;25:816–22.
23. Pierce EM, Reed LR, Shaw WJ, McGrail BP, Icenhower JP, Windisch CF, et al. Experimental determination of the effect of the ratio of B/Al in glass dissolution along the nepheline ($NaAlSiO_4$-malinkoite ($NaBSiO_4$) join. Geochim Cosmochim Acta. 2010;74:2634–54.
24. Lee SK, Stebbins JF. The degree of aluminum avoidance in aluminosilicate glasses. Am Min. 1999;84:937–45.
25. Bista S, Stebbins JF. The role of modifier cations in network cation coordination number increases with pressure in aluminosilicate glasses and melts from 1 to 3 GPa. Am Min. 2017;102:1657–66.
26. Bista S, Stebbins JF, Wu J, Cross TJ. Structural changes in calcium aluminoborosilicate glasses recovered from pressures of 1.5 to 3 GPa: Interactions of two network species with coordination number increases. J Non-Cryst Solids. 2017;478:50–7.
27. Neuville DR, Cormier L, Montouillot V, Florian P, Millot F, Rifflet JC, et al. Structure of Mg and Mg/Ca aluminosilicate glasses: ^{27}Al NMR and Raman spectroscopy investigations. Am Min. 2008;93:1721–31.
28. Edén M. ^{27}Al NMR studies of aluminosilicate glasses. Ann Rep NMR Spectrosc. 2015;86:237–331.and references therein.
29. Kato Y, Yamazaki H, Yoshida S, Matsuoka J, Kanzaki M. Measurements of density distribution around Vickers indentation on commercial aluminoborosilicate and soda-lime silicate glasses by using micro Raman spectroscopy. J. Non-Cryst. Solids. 2012;358:3473–80.

30. Kato Y, Yamazaki H, Itakura S, Yoshida S, Matsuoka J. Load dependence of densification in glass during Vickers indentation test. J Ceram Soc Japan. 2011;119:110–5.
31. Shannon RD. Revised effective ionic radii and systematic studies of interatomic distances in halides and chalcogenides. Acta Crystallogr A. 1976;32:751–67.
32. D'Espinose de Lacaillerie JB, Fretigny C, Massiot D. MAS NMR spectra of quadrupolar nuclei in disordered solids: the Czjzek model. J Magn Reson. 2008;192:244–51.
33. Massiot D, Fayon F, Capron M, King I, LeCalvé S, Alonso B, et al. Modelling one and two-dimensional solid-state NMR spectra. Magn Reson Chem. 2002;40:70–6.
34. Youngman RE, Zwanziger JW. Multiple boron sites in borate glass detected by dynamic magic angle spinning NMR. J Non-Cryst Solids. 1994;168:293–7.
35. Möncke D, Ehrt D, Eckert H, Mertens V. Influence of melting and annealing conditions on the structure of borosilicate glasses. Phys Chem Glasses. 2003;44:113–6.
36. Eckert H. Structural studies of noncrystalline solids using solid state NMR. New experimental approaches and results. NMR-Basic Principles and Progress. 1994;33:125–98.and references therein.
37. Eckert H. Structural characterization of non-crystalline solids and glasses by NMR spectroscopy. Prog NMR Spectrosc. 1992;24:159–293.and references therein.
38. Deshpande RR, Eckert H. Sol–gel preparation of mesoporous sodium aluminosilicate glasses: mechanistic and structural investigations by solid state nuclear magnetic resonance. J Mater Chem. 2009;19:3419–26.
39. Iftekhar S, Leonova E, Edén M. Structural characterization of lanthanum aluminosilicate glasses by ^{29}Si solid-state NMR. J Non-Cryst Solids. 2009;355:2165–74.
40. Jaworski A, Stevensson B, Edén M. Direct ^{17}O NMR experimental evidence for Al-NBO bonds in Si-rich and highly polymerized aluminosilicate glasses. Phys Chem Chem Phys. 2015;17:18269–72.
41. Jäger C, Müller-Warmuth W, Mundus C, van Wüllen L. ^{27}Al MAS-NMR spectroscopy of glasses: new facilities by application of 'SATRAS'. J Non-Cryst Solids. 1992;149:209–17.
42. Medek A, Harwood JS, Frydman L. Multiple-quantum magic-angle spinning NMR: a new method for the study of quadrupolar nuclei in solids. J Am Chem Soc. 1995;117:12779–87.
43. Stebbins JF. Cation sites in mixed-alkali oxide glasses. Correlations of NMR chemical shift data with site size and distance. Solid State Ion. 1998;112:137–41.
44. Ratai E, Chan JCC, Eckert H. Local coordination and spatial distribution of cations in mixed-alkali borate glasses. Phys Chem Chem Phys. 2002;4:3198–208.
45. Watts SJ, Hill RG, O'Donnell M, Law RV. Influence of magnesia on the structure of bioactive glasses. J Non-Cryst Solids. 2010;356:517–24.
46. Kim KS, Bray PJ. ^{11}B NMR studies of glasses in the system Na_2O-MgO-B_2O_3. Phys Chem Glasses. 1974;15:47–51.
47. Sen S, Maekawa H, Papatheodorou GN. Short-range structure of invert glasses along the pseudo-binary join $MgSiO_3$-Mg_2SiO_4: results from ^{29}Si and ^{25}Mg MAS NMR spectroscopy. J Phys Chem B. 2009;113:15243–8.
48. Kroeker S, Neuhoff PS, Stebbins JF. Enhanced resolution and quantitation from 'ultrahigh' field NMR spectroscopy of glasses. J Non-Cryst Solids. 2001;293–295:440–5.
49. Shimoda K, Nemoto T, Saito K. Local structure of magnesium in silicate glasses: a ^{25}Mg 3QMAS NMR study. J Phys Chem B. 2008;112:6747–52.

SUPPORTING INFORMATION

Additional supporting information may be found online in the Supporting Information section.

How to cite this article: Lograd M, Eckert H, Murata T, Nakane S, Yamazaki H. Structure-property relations in crack-resistant alkaline-earth aluminoborosilicate glasses studied by solid state NMR. *J Am Ceram Soc*. 2021;104:2250–2267. https://doi.org/10.1111/jace.17629